

INTRODUCTION

Even with the surge in use of renewable energy, for the foreseeable future the primary energy source for power applications is likely to be fossil fuels. Using these resources as efficiently as possible for both economic reasons and to minimize carbon dioxide emissions is critical (Viswanathan and Bakker, 2000; Viswanathan et al., 2005). In order for power plants to be more efficient they need to run at higher temperature: an operating temperature increase from 873 K to 1073 K would increase the efficiency from <40% to >50%. This requires materials that are strong enough, can withstand an environment that may contain not only steam but also sulfur, display good oxidation and corrosion resistance and are economically viable (Viswanathan et al., 2005). The ultimate goal is to have a material that has a creep rupture stress of 70 MPa for 10⁵ h operating at a temperature of 1073 K (Takeyama, 2007), and eventually at 1143 K (Project 463, 2007).

The martensitic/ferritic alloys that are currently used in power plants are limited to use at operating temperatures \leq 873 K (Viswanathan and Bakker, 2000). Nickel-based superalloys, some titanium alloys, and, possibly, oxide-dispersion strengthened ferritic alloys (Miller et al., 2003, 2005) can satisfy the strength and, at least for nickel-based alloys (Project 463, 2007), the oxidation and corrosion requirements at temperatures \leq 933 K. Unfortunately, these materials are too expensive except for use in specialized applications (Takeyama, 2007). This critical need for advanced materials for steam turbine components in ultra supercritical power plants has been long recognized and forms the basis of efforts in Japan, Europe and the U.S. (Viswanathan and Bakker 2000; Takeyama, 2007).

Recent efforts in this area have focused on devising new austenitic steels strengthened with Laves phases, see **Figure 1** (Maziasz, 1989; Takeyama et al., 2001; Takeyama, 2007; Yamamoto et al., 2007a, 2007b, 2008), whose purpose is to provide a “grain boundary precipitation strengthening mechanism” (Tarigan et al., 2011, 2012). The addition of aluminum can be used to improve oxidation resistance in these alloys (Yamamoto et al., 2005, 2007a, 2007b; Brady et al., 2005, 2007a, 2007b). Such alumina-forming austenitic (AFA) stainless steels have shown promise to decrease our reliance on expensive Nickel-base alloys for aggressive conditions in energy production and chemical processing environments (Brady et al., 2014). AFAs use alumina instead of chromia as a protective oxide scale for high corrosion resistance since it is known to offer even better protection at high temperatures (Kofstas, 1995; Heubner 2000). AFA stainless steels were in development as early as the 1970s (McGurty, 1978) and more recently a new family of AFAs has been under development at the Oak Ridge National Laboratory, ORNL (Yamamoto et al., 2005, 2007a, 2007b, 2008, 2011; Brady et al., 2005, 2007a, 2008; 2014). In the newer grades of AFAs, both B2-structured NiAl and Laves phase precipitates are present on both the grain boundaries and in the austenitic matrix, and MC precipitates or L1₂-structured Ni₃Al precipitates are used to increase the creep strength (Brady et al., 2014; Yamamoto et al., 2008; 2011). While great strides have been made in these AFA stainless steels optimization of their properties has been difficult because the effects that different alloying elements and precipitates have on their creep strength is not understood. The AFA stainless steels studied encompass a wide range of compositions and continued study of this system is needed to find the optimal combination of alloying elements that provide the best creep strength and oxidation resistance with a balance of cost for future commercialization (Brady et al., 2014).

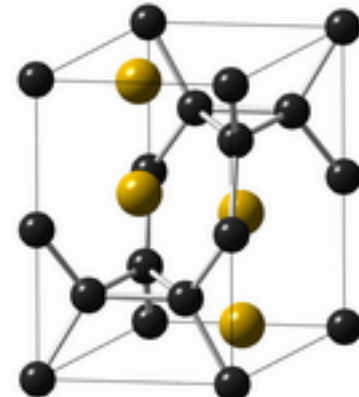


Figure 1. Hexagonal C14 Laves phase structure adopted by many AB₂ intermetallic compounds. The large yellow spheres represent “A” atoms and the smaller black spheres represent “B” atoms.

The purpose of this proposal and the **intellectual merit of the proposed activity** is to understand the high temperature deformation behavior of AFA stainless steels and elucidate the role of the different precipitates and solute additions on the creep strength. The work will focus on the model alloy Fe-20Cr-30Ni-2Nb-5Al. This was chosen because it can be fully solutionized upon annealing at 1523 K and because we have experience with it in our current project. While working on a specific alloy, the precipitation phenomena and deformation behavior that will be studied have applicability to many alloy

systems. It is worth noting that the proposed work is not an alloy development effort, but is focused on fundamental work that will aid further development (by others) of precipitate-strengthened austenitic alloys. The work will involve several collaborations: with Prof. Min Song, Central South University, Changsha, PRC on creep testing; with Prof. Simon P. Ringer, University of Sydney, Sydney, Australia on Atom probe tomography (APT); and with Prof. Paul R. Munroe, University of New South Wales, Kensington, Australia on using an electron probe microanalyzer (EPMA).

FURTHER BACKGROUND

Laves-Phase Strengthened Austenitic Stainless Steels

Takeyama et al. (2001) systematically studied Laves phase precipitation in the austenitic Fe-20Cr-(25-40)Ni-2Nb (in at. %) quaternary alloy system. The precipitates, which adopt the hexagonal C14 structure, are often referred to as the ϵ phase. For alloys containing 35 at. % Ni, the precipitates are elongated with many interfacial dislocations, whereas for alloys containing 25 at. % Ni the precipitates are smaller and more equi-axed. In these Fe-Cr-Ni-Nb alloys, the c/a ratio of the precipitates decreases as the Ni content decreases for 15-25 at. % Ni and changes little with further increases in Ni content. At 25 at. % Ni the c/a ratio is about the same as that of binary stoichiometric Fe_2Nb at 1.63, which is near the value for the cubic symmetry C15 Laves structure. Although the precipitates are referred to by Takeyama (2007) as Fe_2Nb , they contain 14-15 at. % Cr, 26 at. % Nb and 17-25% Ni, depending on the overall alloy composition. Takeyama (2007) determined TTT curves for the precipitates and found that precipitation at 1173-1273 K occurred first on the grain boundaries after ~ 300 s, but only after >1000 s in the matrix. After long ageing times (4.32×10^6 s) the precipitates on the *grain boundaries* became significantly larger ($\leq 3 \mu\text{m}$).

In contrast, Yamamoto et al. (2007b) found that the ϵ Laves phase precipitates in the *matrix* of the alloy Fe-15Cr-20Ni-(1-2)Nb were relatively stable during both ageing and creep testing at 1073 K. This stability may arise partly from the semi-coherent interface of the Fe_2Nb precipitates, as indicated by the strain contrast present in transmission electron microscope (TEM) images even after long-term annealing (Takeyama, 2007), and also from the presence of small additions of Al, Mo, C and B. Small elemental additions have also been shown to stabilize Laves phases in other systems: Maziasz (1989) noted that Si additions led to the formation of $\text{Fe}_2(\text{Mo},\text{Nb})$ precipitates in austenitic alloys, while Yamamoto et al. (2008) found that small Zr additions promote Fe_2Ti Laves phase precipitates.

Yamamoto et al. (2008) studied the microstructural evolution of Fe-20Cr-30Ni-2Nb alloys with and without additions of 0.4 Si, 0.2 Zr or 5.0 Al (in at. %) during creep at 1023 K and 100 MPa. The Si addition helped to both refine the particle size (from $\sim 1 \mu\text{m}$ to 300 nm) and produce a greater volume fraction of particles during ageing at 1073 K, and stabilized them against coarsening, resulting in superior creep resistance. Interestingly, alloys that were only *solution treated* showed superior creep properties to those that were *aged* prior to creep testing. The authors speculated that this phenomenon was because the particles that were dynamically precipitated during creep were finer (300-400 nm) and, thus, more effective at pinning dislocations. The Zr addition improved the creep resistance more dramatically than the Si additions possibly by stabilizing very fine δ - Ni_3Nb particles. The addition of Al not only improved the creep resistance due to the formation of 30 nm diameter Ni_3Al precipitates, but also improved the oxidation through the formation of a protective alumina layer on the surface.

The fundamental issues with the use of austenitic alloys for high temperature applications were articulated by Yamamoto et al. (2008) who noted that "The strengthening effect of Fe_2Nb (Laves phase) strongly depends on its size and volume fraction, indicating that the thermal stability of the particle size and distributions is the key to improve creep properties." More specifically, the two key issues are that: 1) the increase in size and density of the large Laves phase particles that develop on the grain boundaries during creep testing (Yamamoto et al. 2008) will ultimately result in specimen failure when the grain boundary coverage of these brittle particles is large enough; and 2) further refinement of the Laves phase precipitates to ~ 100 nm dia. is necessary to improve the creep strength Yamamoto et al. (2008).

Recently, Tarigan et al. (2011, 2012) examined the effect of boron (0.03%) on the creep strength of Fe-20Cr-30Ni-2Nb (in at. %). Both the boron-doped and boron-free alloys with contained Ni_3Nb precipitates (the γ phase at short annealing times and the δ phase at long times) within the grains and Laves phase

precipitates on the grain boundaries. The boron decreased the creep rate and increased the creep rupture life by a factor of almost four. The role of boron appeared to be to increase the extent of the Laves phase precipitation at the grain boundaries. Simply aging the *boron-free* alloy to increase the extent of grain boundary coverage by the Laves phase from 52% to 89% also increased the creep rupture life and decreased the creep rate to a similar extent as the boron addition. That even with 89% grain boundary coverage by the Laves phase precipitates a creep rupture strain of 77% was attained shows that the precipitates don't necessarily embrittle the alloy. Tarigan et al. (2011, 2012) found that the creep rate, $\dot{\epsilon}$, was related to the area fraction covered by the grain boundary Laves phase, ρ , according to:

$$\dot{\epsilon}/\dot{\epsilon}_0 = (1 - \rho) \quad - (1)$$

$\dot{\epsilon}_0$ is the creep rate when $\rho = 0$. They suggested that the role of the grain boundary phase was to suppress deformation at the grain boundaries.

Chen et al. (2014) also studied Fe-20Cr-30Ni-2Nb with and without 0.03% B and found that boron both increased the extent and produced finer Laves phase precipitates on the grain boundaries, but by <10% after their longest anneal of 24h, when the grain boundary coverage in the B-doped alloy was ~80%. Using an EPMA, they showed strong boron segregation to the grain boundaries. They found that for both the boron-doped and boron-free alloy, longer aging times prior to creep testing increased the creep life (by up to 100% for a 4h versus a 12 h anneal), and that for the same aging time boron doping increased the creep life (by up to 44% for short aging times but by less at long aging times) by producing greater grain boundary coverage of the Laves phase. Chen et al.'s (2014) results were very similar to those of Tarigan et al. (2011, 2012). Essentially, boron appears to reduce the annealing time to obtain a large grain boundary coverage by the Laves phase.

Alumina-Forming Austenitic Stainless Steels

Even within particular grades of AFAs, the influence of particular precipitate phases on creep strength is complex. A wide variety of creep strengths can be obtained with relatively small changes in alloying elements and phases that are beneficial in some AFAs appear to cause decreased creep strength in others. There are generally three grades of AFAs that have been investigated by the ORNL group based on their nickel content, *viz.*, 20-25Ni, 12Ni, and 32Ni. The 12Ni grade alloys substitute Mn for some of the Ni both to stabilize the austenite relative to the deleterious δ -Fe phase formation and to lower the cost. Unfortunately, this grade has been shown to have relatively poor creep resistance although the reason for the decreased creep strength is poorly understood (Brady et al., 2014; Yamamoto et al., 2011). In 20-25 Ni grade alloys it has been found that the total weight fraction of carbide phases is important. For example, in a 20-25Ni grade alloy with 2.53 wt. % Nb and 0.201 wt. % C there was little MC supersaturation and it showed poor creep resistance compared to 25Ni grade alloys with 1 wt. % Nb and 0.1 wt. % C. It is believed that the 2.53 wt. % Nb alloy showed poorer creep strength because the 2.53 wt. % Nb addition decreased the supersaturation of MC carbides (Brady et al., 2014). The 1 wt. % Nb and 0.1 wt. % C additions have been shown to be the optimal amounts for MC carbide strengthening in other studies of AFAs as well (Brady et al., 2008; Yamamoto et al., 2009). While increasing the Nb content from 1 wt. % to 2.5 wt. % seemed to have a detrimental role on the creep strength for a 25Ni alloy, in the 32Ni grade alloys with 3.3 Nb wt. %, superior creep strength has been observed at 650°C, a feature that appears to be due to strengthening from $L1_2$ Ni_3Al precipitates, producing a creep strength almost five times greater than the best carbide strengthened 20-25 Ni alloy. While the $L1_2$ Ni_3Al improved the creep properties of the 32Ni alloy, at 650°C it is believed that the metastable $L1_2$ Ni_3Al caused the decreased rupture time observed in a 25Ni-4Al-1Nb alloy with increased C content compared to a 25Ni-3Al-1Nb alloy. Although the creep strength was promising there was a tradeoff with significantly reduced creep elongation in the 32Ni grade alloy, which is thought to be due to σ -phase formation. At 750°C, the 32Ni alloy creep results were comparable to those of both the 20-25Ni and 12Ni alloy grades (Brady et al., 2014).

32Ni grade alloys with decreased chromium content (14 wt. % versus 19 wt. %) and additional alloying elements such as Zr and Ti have less σ -phase formation and improved creep properties. Indeed, a Zr, Ti alloyed 32Ni alloy with additions of carbon and boron was shown to have a creep-rupture life that exceeded that of the commercially-available Fe-base alloy A286 by an order of magnitude (Yamamoto, Muralidharan, Brady, 2013). Boron improves the creep properties of AFA stainless steels, but why is not

understood. Unlike the Al-free Fe-20Cr-30Ni-2Nb alloy studied by Tarigan et al. (2011, 2012) and Chen et al. (2014), the addition of boron to a 32Ni grade alloy did not seem to have a significant effect on grain boundary precipitation, and in this case it was hypothesized that the boron addition formed a strain field in the matrix that increased resistance to creep deformation (Yamamoto, Muralidharan, Brady, 2013). It is worth noting that unlike the Al-free alloys in which a solutionizing anneal can completely dissolve the Laves phase precipitates, in the more complex alloys developed at ORNL solutionizing anneals still leave substantial volume fractions of the Laves phase in the material (Yamamoto, Muralidharan, Brady, 2013; Brady et al., 2014, Hu et al., 2014).

While computational methods have helped to design AFA alloys to limit the formation of deleterious phases, such as the sigma phase, and to help stabilize the austenitic matrix, it is clear that the additions of small alloying elements and their effect on the properties of AFA stainless steels require more detailed microstructural characterization. Even with an understanding of what phases may be present, creep mechanisms in this system are not well enough understood to predict which potential strengthening precipitate will be most beneficial for creep strength. For many of the AFA alloys that were also tensile tested, the creep and elevated temperature tensile properties did not correlate well. For example in the 20-25 Ni grade alloys while B2-NiAl and Laves precipitation improves tensile properties, MC carbides appear to show a stronger influence on the creep strength (Brady et al, 2014; Yamamoto et al., 2011). The ORNL group also questioned whether the Laves phase had any significant influence on the creep strength (Bei et al., 2010). The lower tensile strength they observed at 1023K compared to room temperature appeared to be due to the softening of the B2 NiAl phase which produces significant strengthening at room temperature.

In this work we are studying the effects of cold work on the simplified AFA stainless steel Fe-20Cr-30Ni-2Nb-5Al (at. %) – many of the alloys studied by the ORNL Group are much more complex containing 10 or so elements (Brady et al., 2014). Cold rolling was performed after solution treatment at 1523 K to 25%, 50% and 90% rolling reduction with subsequent ageing performed for various times at 973K, 1073K and 1173 K. A significant density of dislocations was found in the matrix in the solutionized and aged specimens even without cold rolling, possibly due to the punching out of dislocations from around the precipitates during cooling, see **Figure 2**.

We found that cold work accelerated the precipitation kinetics of both C14-type Fe_2Nb -type Laves phase and B2-type NiAl precipitates markedly compared to simply aging, presumably due to heterogeneous precipitation on dislocations, see **Figure 3**. It is worth noting that in the material that was simply aged the Laves phase precipitates nucleate before the B2 precipitates, but it is no longer clear that this sequence occurs after cold work and aging, see **Figure 3**. While often co-located, these two types of particles are distinct, see **Figure 4**. L1_2 (ordered f.c.c.) precipitates were also observed in samples aged at 973K with 90% prior cold work, see **Figure 5**, but not in specimens annealed at 1073K, which is in line with thermodynamic calculations. The additional fine L1_2 precipitates present at 973K are presumably the reason for the greater hardness of the 973K-annealed material, see **Figure 6**. We have shown using APT that the L1_2 precipitates are $\text{Ni}_3(\text{Al},\text{Ti})$, see **Figure 7**.

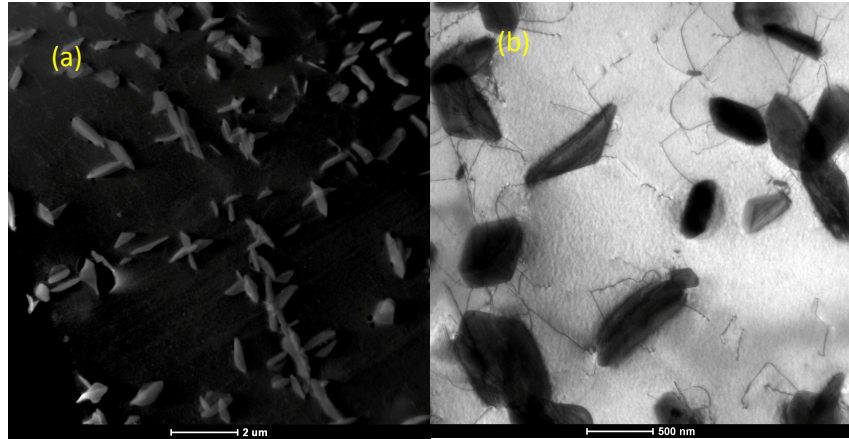


Figure 2. (a) Dark field scanning transmission electron micrograph showing Laves phase precipitates in Fe-20Cr-30Ni-2Nb-5Al solution treated at 1523 K and aged at 1073 K for 240 h, and (b) bright field TEM image showing dislocations associated with the precipitates, presumably punched out during cooling due to the thermal mismatch. From P.R. Munroe, G. Rayner and I. Baker, unpublished research.

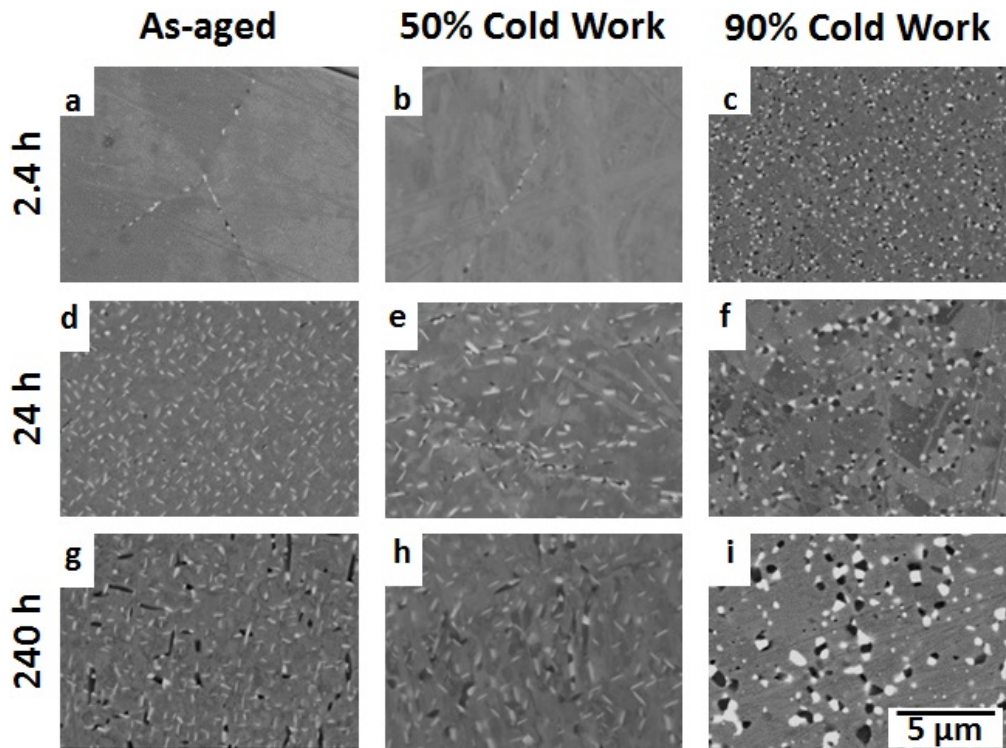


Figure 3. Backscattered electron images from specimens aged at 1073K: a) 2.4 h; b) 2.4 h after 50% cold work; c) 24 h after 90% cold work; d) 24 h; e) 24 h after 50% cold work, 24 h; f) 240 h after 90% cold work; g) 240 h; h) 240 h after 50% cold work; and i) 240 h after 90% cold work. The particles with light contrast are the Laves phase; the particles with dark contrast are NiAl. After Trotter et al., 2014.

Compared to material that had not been strained, defects introduced by 50% and 90% cold work at 973K and 1073K not only caused a more rapid precipitation in the matrix but also an increase in the total volume fraction of precipitates as compared to material that had been simply aged, see Figure 3. Histograms of the particle size distributions were produced for each annealing time and temperature (not shown here), and as might be expected they were log-normal with the particle size increasing steady with increasing time and increasing temperature (Trotter et al., 2014).

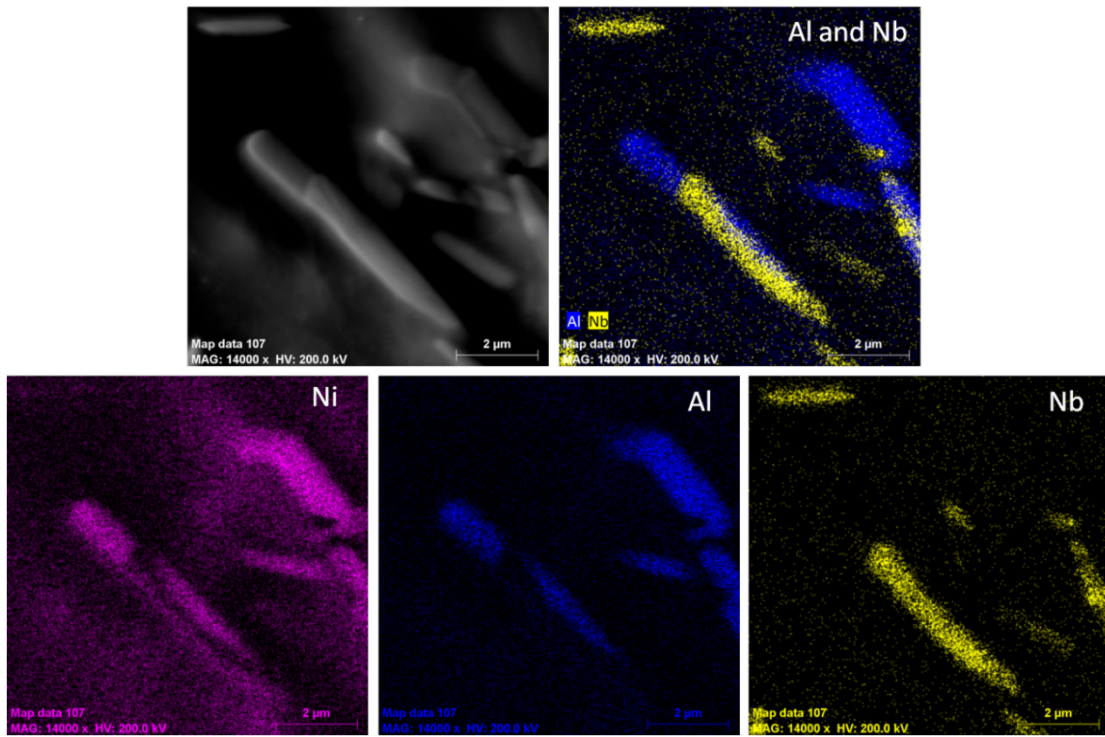


Figure 4. Energy dispersive X-ray maps of Ni, Al, and Nb from 50% cold-rolled Fe-20Cr-30Ni-2Nb-5Al aged at 1073 K for 240 h taken across the region shown in dark field scanning transmission electron micrograph image (top left). The Al and Nb maps are overlayed to show that the two types of precipitates (Laves and B2), while often co-located, are distinct. Munroe, Rayner and Baker, unpublished research.

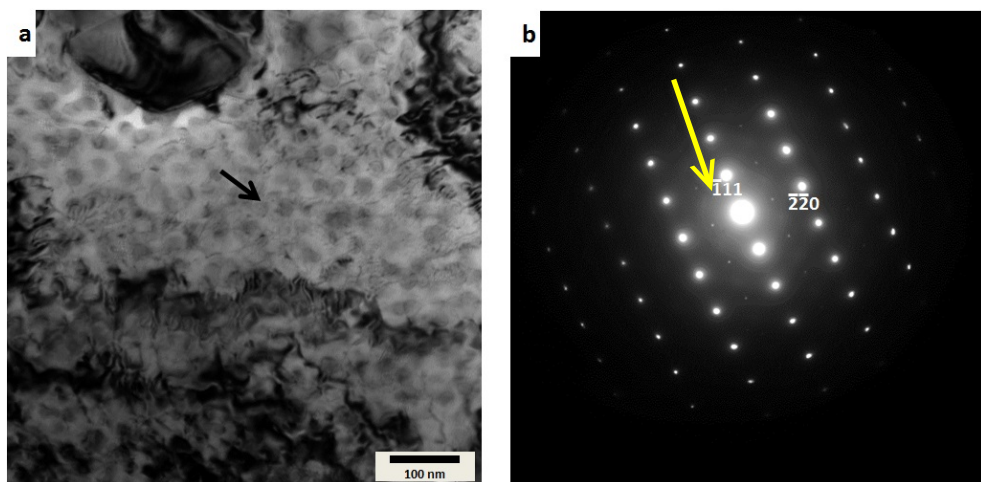


Figure 5. a) Bright field TEM image of Fe-20Cr-30Ni-2Nb-5Al after 90% rolling reduction and aged 240 h at 973K; b) selected area diffraction pattern from area arrowed in a) showing $L1_2$ superlattice reflections (arrow points to a systematic row of $L1_2$ superlattice reflections). After Trotter et al., 2014.

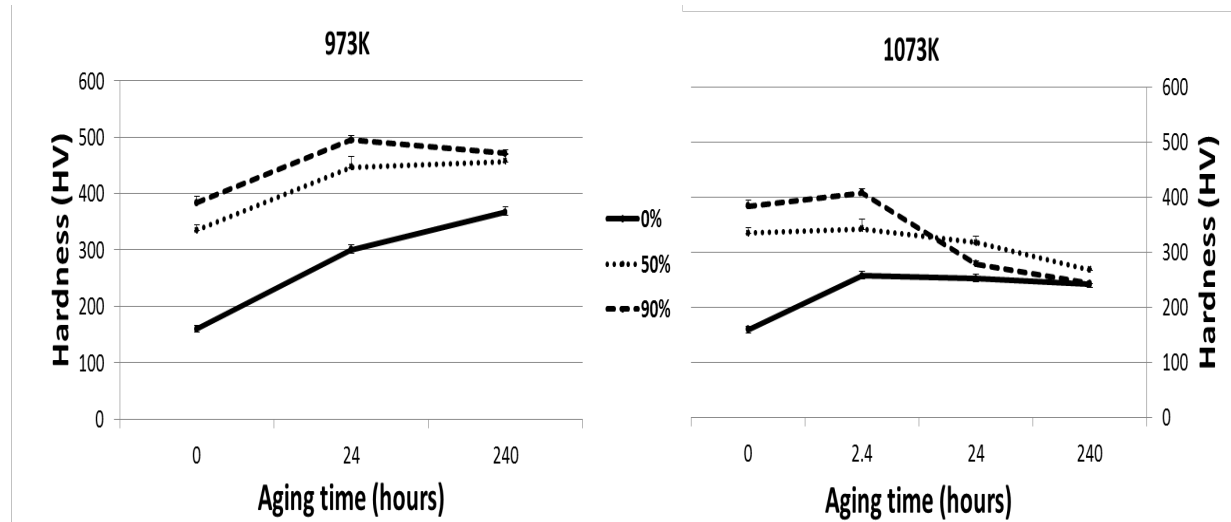


Figure 6. Hardness for samples annealed at 973K and 1073K after 0%, 50% or 90% cold rolling reduction.

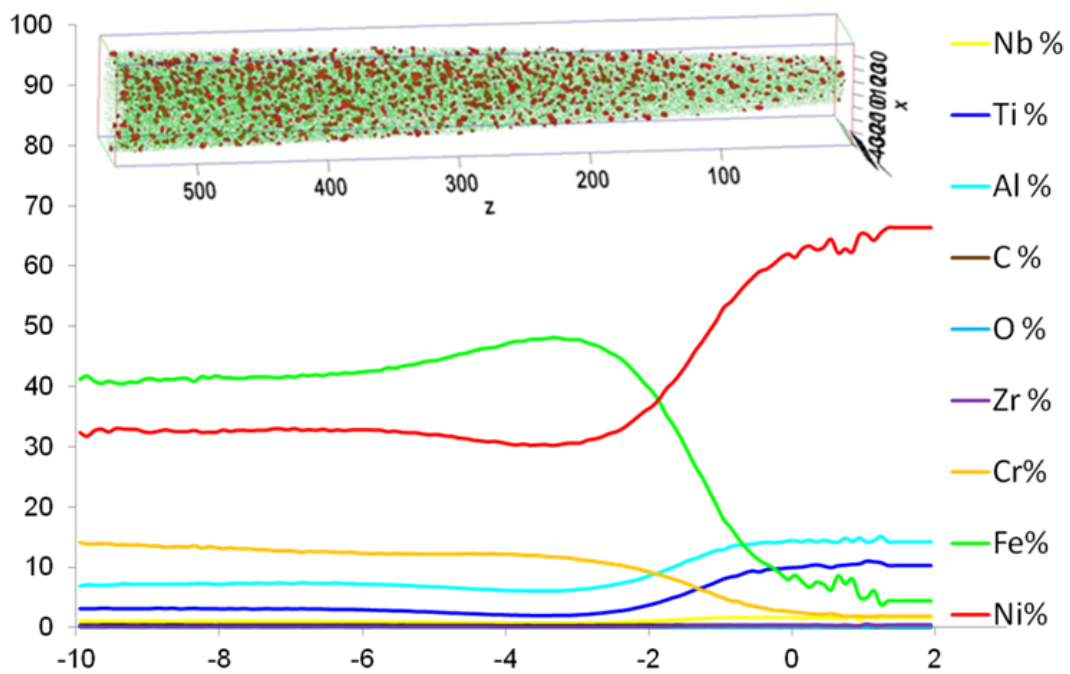


Figure 7. Atom probe analysis of as-received ORNL alloy DAFA26. The curve shows the elemental distributions across the interface between a Ni_3Al precipitate and f.c.c iron matrix. The upper inset shows a reconstruction showing the Ni_3Al precipitate distribution. After Hu et al., 2014.

Similar to the accelerating effects of a boron addition on the Laves phase precipitation in Al-free Fe-20Cr-30Ni-2Nb observed by Tarigan et al. (2011, 2012) and Chen et al. (2014), we have found that the addition of silicon to an AFA-type alloy with a composition that despite having less Laves phase forming Nb (Fe-15Cr-23Ni-1.5Nb-7Al-0.2Si at. %) has increased precipitation kinetics, decreased precipitate size and an increase in the overall volume fraction of precipitates, in this case of both the Laves phase and NiAl precipitates (Trotter and Baker, unpublished), see **Figure 8**. As noted earlier, Yamamoto et al. (2008) found that Si additions produced a decrease in precipitate size and a greater volume fraction of

precipitates.

Figure 8. Backscattered electron images showing the effects of aging at 973K on precipitation in AFA-type alloys with (top row) and without (bottom row) the addition of 0.2% Si. The particles with light contrast are the Laves phase; the particles with dark contrast are NiAl. Trotter and Baker, unpublished research.

We have also examined the effects of simply aging on the room temperature tensile properties of Fe-20Cr-30Ni-2Nb-5Al and the results are quite dramatic, see **Figure 9**. After solutionizing for 24 h at 1523K the segregated as-cast microstructure was no longer visible and all the Laves phase precipitates had completely dissolved, see **Figure 10**. This material showed a yield strength of 205 MPa, an elongation to failure of 52% and a low work hardening rate of 256 MPa.

An anneal of 2.4 h at 1073K produced substantial coverage along the grain boundaries of fine alternating Laves phase and NiAl precipitates, but little obvious precipitation in the grains. This heat treatment produced a 57% increase in yield strength to 322 MPa with an increase in work-hardening rate, and a slight reduction in elongation to failure to 37%. It is noteworthy that for this heat-treatment there is a clear yield drop and a long Lüders region, see **Figure 9**.

Subsequent anneals increase the size and volume fraction of the precipitates both in the grain and on the grain boundaries, and lead to almost complete coverage of the grain boundaries after a 1325 h anneal, see **Figure 10**. These changes increase the yield strength and decrease the elongation, see **Figure 9**. The Lüders region on the stress-strain curves also disappears for the longer anneals. Interestingly, even though the grain boundaries are completely covered in brittle NiAl and Laves phase precipitates after the 1325h anneal, the material can still show 19% elongation.

We found that the orientation relationship between the Fe_2Nb Laves phase precipitates and the austenite matrix was $(0001)_{\text{Fe}_2\text{Nb}} \parallel (111)_{\gamma}$: $[10\bar{1}0]_{\text{Fe}_2\text{Nb}} \parallel [\bar{1}10]_{\gamma}$, as proposed by Denham and Silcock (1969). The B2 precipitates appear to show the Kurjumov-Sachs relationship with the matrix. In ongoing work, we are examining how cold work and aging affect the room temperature tensile properties.

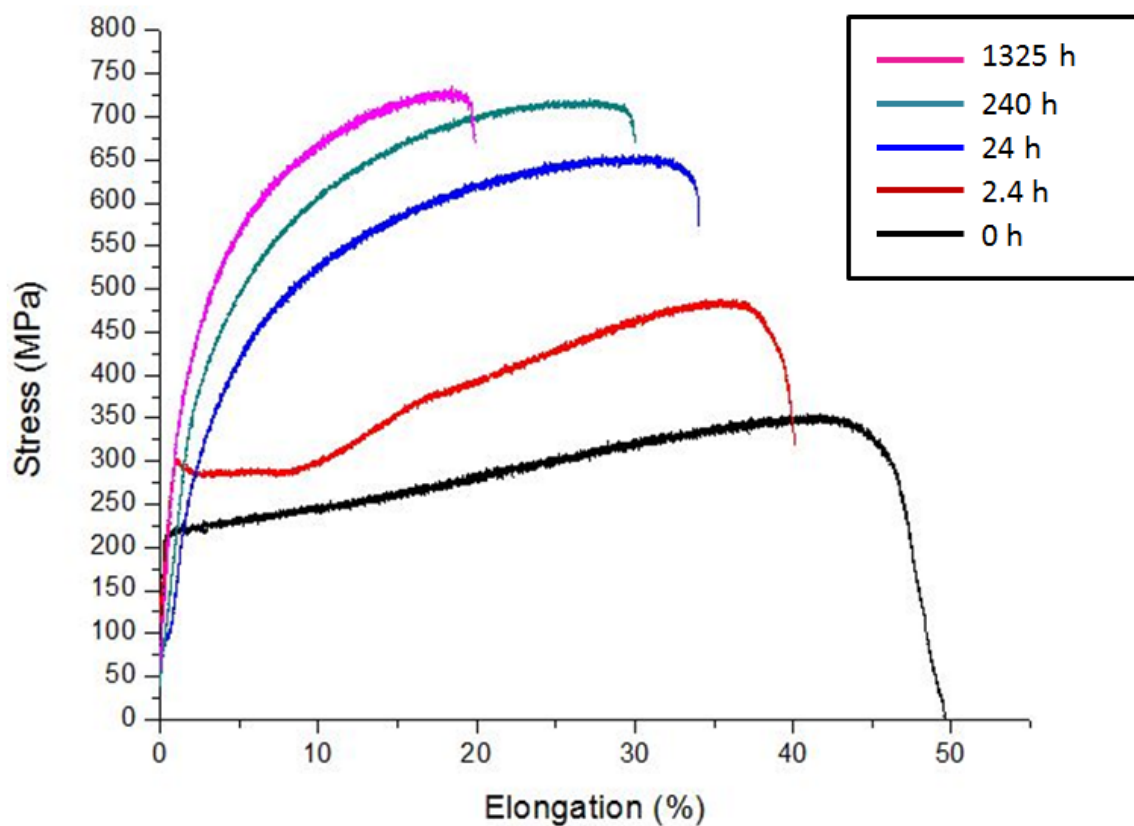


Figure 9. Representative tensile curves of Fe-20Cr-30Ni-2Nb-5Al (at. %) homogenized at 1523K for 24 h and subsequently aged at 1073K for the different times as indicated.

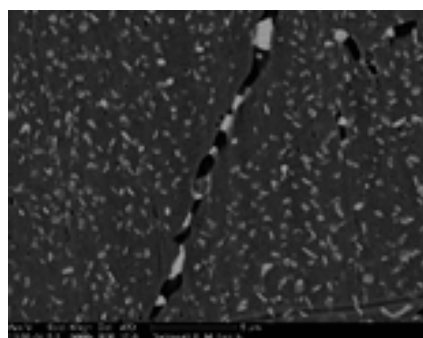


Figure 10. Backscattered electron images showing grain boundary precipitation in Fe-20Cr-30Ni-2Nb-5Al (at. %): (a) after a homogenization anneal; and aged at 1073K for b) 2.4 h, c) 24 h, d) 240 h and e) 1325h. The particles with light contrast are the Laves phase; the particles with dark contrast are NiAl.

QUESTIONS

As noted above the best current AFA stainless steel (referred to as 32ZCB) - 14Cr, 32.5Ni, 3Al, 0.14Si, 3Nb, 1.9Ti, 0.3Zr, 0.065C, 0.005B (in wt. %), balance Fe – which has L₁₂ Ni₃(Al,Ti), B₂ (Ni,Fe)Al and C14 Fe₂(Nb,Ti) Laves phase precipitates, has a creep-rupture life at a temperature of 1023K and a stress of 100 MPa that is an order of magnitude longer than that of the commercial iron-based superalloy A286 (Yamamoto, Muralidharan, Brady, 2013). While great progress has been made in the development of AFA stainless steels over the last few years, how the different precipitates and solutes control the high temperature strength is poorly understood. Based on the work presented above, there are some specific questions about effects of various components on the strength of AFA stainless steels:

1. Does the Laves phase affect the creep strength of AFA stainless steels? It is clear that the creep rate is related to the grain boundary coverage in Al-free Laves phase strengthened stainless steels (Tarigan et al. 2011, 2012; Chen et al., 2014), but whether the Laves phase precipitates contribute to the creep strength in AFA stainless steels in which fine L₁₂ precipitates provide substantial strengthening is unclear (Bei et al., 2010).
2. Do aged alloys show better creep properties than simply solutionized alloys? Note that Yamamoto et al. (2008) found that *solution treated* Fe-20Cr-30Ni-2Nb alloys with and without additions of 0.4 Si, 0.2 Zr or 5.0 Al (in at. %) crept at 1023 K and 100 MPa showed superior creep properties to those that were simply *aged* prior to creep testing, possibly because the particles that dynamically precipitated during creep were finer (300-400 nm) and, thus, more effective at pinning dislocations.
3. How does boron increase the creep life? For Al-free alloys, it simply appears to increase the Laves phase precipitation kinetics (Tarigan et al. 2011, 2012; Chen et al., 2014). Why boron increases the creep life in more complex AFA stainless steels that contain several different kinds of precipitates is unclear (Yamamoto, Muralidharan, Brady, 2013).
4. Is there any correlation between the room temperature or elevated temperature strength of various AFA stainless steels and their creep properties? A reason that there may not be is because the strengthening mechanisms can be quite different between room temperature and elevated temperature and because some alloys show dynamic strain aging (DSA) at elevated temperatures, see **Figure 11**.

Figure 11. Stress-strain curves for the ORNL alloy DAFA 29 tensile tested at 973K at two different strain rates. The DAFA 29 had an analyzed composition (wt. %) of 13.83Cr, 0.13 Mn, 32Ni, 0.12Cu, 3.02Al, 0.15Si, 2.87Nb, 2Ti, 0.1Mo, 0.32Zr, 0.11C, 0.001B, balance Fe. B. Hu and I. Baker, unpublished research.

PROPOSED RESEARCH

The research proposed here will attempt to elucidate the high temperature strengthening mechanisms in AFA stainless steels, and in particular we will attempt to answer the questions posed above. The work will use the model alloy Fe-20Cr-30Ni-2Nb-5Al with and without 0.03% boron, which we have worked on previously and which can be fully solutionized upon annealing at 1523 K. A schematic of the microstructural features of the Laves phase-strengthened alumina-forming austenitic stainless steel is shown in **Figure 12**.

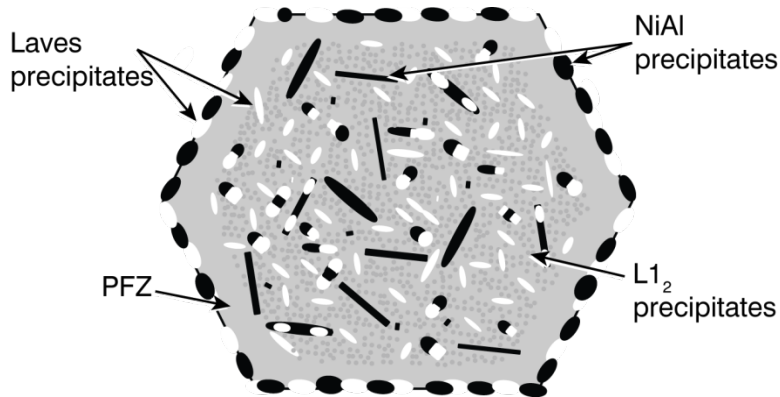


Figure 12: Schematic of the microstructure of a Laves phase-strengthened alumina-forming austenitic stainless steel. The f.c.c. matrix contains L₁₂, B₂ and Laves phase precipitates, while Laves phase precipitates and B₂ precipitates also form along the grain boundaries. There is also a precipitate free zone (PFZ) along the grain boundaries.

We will undertake four series of elevated temperature mechanical tests as outlined below. In each series of tests, the microstructure will be carefully analyzed using a variety of techniques (see later) both before and after high temperature testing. A summary of microstructures examined in these series of tests is listed in **Table 1** (some of these tests overlap with others).

1. We will anneal Fe-20Cr-30Ni-2Nb-5Al for various times at 973K to produce different amounts of coverage of the Laves and NiAl precipitates along the grain boundaries, see **Figure 10**, and perform creep testing on the resulting material. (L₁₂ precipitates are also present after annealing at 973K.) In this work, we will test the applicability of the empirical equation determined by Tarigan et al. (2011, 2012) and corroborated by Chen et al. (2014) that the strain rate, $\dot{\epsilon}$, decreases with increasing coverage of the grain boundaries by precipitates, p , according to: $\dot{\epsilon}/\dot{\epsilon}_0 = (1-p)$. A key difference from the work of Tarigan et al. (2011, 2012) and Chen et al. (2014) is that in their work the grain boundary precipitates were *only* Laves phase (since their alloys did not contain Al), whereas the alloy tested here will have alternating Laves phase and B₂ precipitates, and the latter will be soft at the test temperature. The extent of grain boundary coverage will be carefully determined.
2. We will compare the creep properties of the as-homogenized, fully solutionized base alloy, in which B₂, Laves phase and L₁₂ precipitation will occur during testing, with that of the 973K annealed alloys noted above that contain B₂, Laves phase and L₁₂ precipitates. In addition, we will anneal two specimens (24 h, 1325 h) at 1073K, which will contain B₂ and Laves phase precipitates, in which L₁₂ precipitation will occur during mechanical testing. One might expect that during creep testing both the fully solutionized alloy and the alloys initially without the L₁₂ precipitates will show initial higher creep rates but that once precipitation occurs the creep rates will slow down. If finer precipitates are produced by creep testing rather than through simple aging, as suggested by Yamamoto et al. (2008), then we would expect the creep rate to be less for the as-homogenized alloy and the samples annealed at 1023K than the alloys in which 973 K aging was used to produce precipitates before creep testing. We will perform several interrupted creep tests on the as-solutionized and the aged alloys and analyze the microstructure using a scanning electron microscope (SEM) and a TEM in order to examine the microstructural evolution during creep.

We will perform creep tests in which we compare the effects of precipitation during creep by varying the presence of B₂, Laves phase, and L₁₂ in the starting microstructure. In the base case we will start from the fully solutionized base alloy, expecting all three precipitates to precipitate out during

creep. We will then start from a 973K anneal where all precipitates are already present in the matrix before testing begins. Finally we will start from a 1073K anneal (24 h, 1325 h) with just Laves and B2 precipitates present in the starting microstructure and observe how subsequent L1₂ precipitation affects creep properties. One might expect that during creep testing both the fully solutionized alloy and the alloys initially without the L1₂ precipitates will show initial higher creep rates but that once precipitation occurs the creep rates will slow down. If finer precipitates are produced by creep testing rather than through simple aging, as suggested by Yamamoto et al. (2008), then we would expect the creep rate to be less for the as-homogenized alloy and the samples annealed at 1023K than the alloys in which 973 K aging was used to produce precipitates before creep testing. -mortem analysis of the crept samples will be analyzed using a scanning electron microscope (SEM) and a TEM to study precipitation effects.

3. We will compare the creep behavior of Fe-20Cr-30Ni-2Nb-5Al with and without 0.03% B after different anneals at 973K. We will determine whether the boron addition increases the precipitation kinetics as in the similar but Al-free alloys studied by Tarigan et al. (2011, 2012) and Chen et al. (2014). The key question is whether boron reduces the creep rate and increases the creep life and, if so, whether this is simply due to increased precipitation at the grain boundaries. We will determine the segregation of boron using EPMA and APT, in particular whether the boron is associated with the grain boundary, the B2 precipitates or the Laves phase precipitates.
4. We will compare several specimens of Fe-20Cr-30Ni-2Nb-5Al with and without 0.03% B either simply aged or cold-worked and aged to give different room-temperature mechanical properties and tensile test them at different strain rates at 973K to determine if dynamic strain aging occurs. We will then perform creep tests to determine if we can relate the creep behavior to the displacement-controlled tensile tests performed at room temperature or at 973K.

Table 1. Materials, processing conditions (after solutionizing at 1523K), resulting microstructures and tests series for the base Fe-20Cr-30Ni-2Nb-5Al alloy and with additions of 0.03% B boron.

Material	Processing	Microstructural Feature	Series
base	As homogenized	No precipitates present.	1, 2, 4
base	Age 2.4 h, 24 h, 240 h, 1325 h @ 973K	Different amounts of B2, Laves phase and L1 ₂ precipitation.	1, 2, 3, 4
base	Age 24h, 1325 h @ 1073K	Different amounts of B2 and Laves phase precipitation.	2
+ boron	Age 0, 2.4 h, 24 h, 240 h, 1325 h @ 973K	Different amounts of B2, Laves phase and L1 ₂ precipitation.	3
base	90% cold rolling reduction; age 24 h, 1325 h @ 973K	Different amounts of B2, Laves phase and L1 ₂ precipitation.	4
+ boron	90% cold rolling reduction; age 24 h, 1325 h @ 973K	Different amounts of B2, Laves phase and L1 ₂ precipitation.	4

Casting

Alloys of Fe-20Cr-30Ni-2Nb-5Al with and without boron will be produced by arc-melting from elemental constituents under an argon atmosphere. Each alloy will be flipped over and remelted twice to ensure homogeneity, following our standard practice. After a solutionizing treatment at 1523K a material with a grain size of ~800 μm is obtained. The compositions of the ingots will be confirmed using an EPMA via a collaboration with Prof. Paul R. Munroe of the University of New South Wales, Australia, a collaborator for over twenty years. The boron content of the ingots will be determined via chemical analysis using a commercial vendor.

Microstructural Analysis

Microstructural characterization of the alloy will be performed using a combination of state-of-the-art techniques and instruments both *before* and *after* testing. To fully characterize the microstructure of the precipitate structure of Fe-20Cr-30Ni-2Nb-5Al-(B), the following parameters will be determined:

- precipitate size and spacing.
- lattice parameters of the phases, and, hence the misfit parameters and interface strains;
- microchemistry of and around the precipitates.

Four techniques will be used for microstructural characterization:

- We will use a Rigaku rotating anode X-ray set to precisely measure lattice parameters.
- Backscattered electron imaging on FEI XL30 field emission gun (FEG) SEM will be used to get an overview of the precipitate size and distribution, as performed in Trotter et al. (2014).
- Conventional diffraction-contrast TEM will be performed on a FEI Tecnai FEG 200 keV TEM to determine the details of the morphology of the phases. Energy dispersive spectroscopy (EDS) and both selected area diffraction (SAD) and convergent beam electron diffraction (CBED) analysis will also be performed using this instrument to obtain the chemistry and orientation relationships of the phases. Higher Order Lower Zone line shifts in the transmitted disc in CBED patterns will be used to assess strains in the phases.
- APT will be utilized to examine the grain boundary chemistry. Grain boundary specimens will be cut out using a FEI Nova 200 Nanolab focused ion beam microscope (FIB) using lift-out and annular milling methods [Miller, 2000]. The resulting specimens, will be examined with a voltage-pulsed Imago Scientific Instruments local electrode atom probe (LEAP®), which provides high-speed data acquisition over a large field of view, at the University of Sydney, Australia through a long time collaborator Prof. Simon P. Ringer. We will also determine whether the boron is associated with a particular type of precipitate at the grain boundaries.
- In collaboration with Prof. Paul R. Munroe, an EPMA located at the University of New South Wales, will also be used to obtain determine whether boron segregates to the grain boundaries as observed by Chen et al. (2014).

Mechanical Testing

Mechanical Testing will take two forms, viz, displacement-controlled tensile tests and constant-stress creep tests. Tensile tests will be performed for test series 4 noted above at 973K at a range of strain rates from $1 \times 10^{-6} \text{ s}^{-1}$ to 1 s^{-1} in air, in order to examine the strain rate sensitivity, including determining whether dynamic strain aging occurs.

We will perform constant-stress creep tests for all the test series noted above at 973K at a stress of 140 MPa in air. Most reported tests of AFA stainless steels have been at temperature from 923-1033K and at stresses from 100-250 MPa, the higher stresses being associated with testing at lower temperatures. We chose 973K and 140 MPa since this will allow direct comparison to the Al-free Laves phase strengthened stainless steels studied by Tarigan et al. (2011, 2012). This temperature is also one of likely first commercial use. While the stress is somewhat higher than the stress that the alloys might be used at, it will result in creep tests that lead to failure in a reasonable length of time (a few hundred hours). Most creep testing will be performed at Dartmouth on a home-built constant-stress creep rig, whose design was based on that of Garofalo, Richmond and Domis (1962). However because of the length of time creep tests require, Prof. Min Song at Central South University, Changsha, PRC will also perform some creep tests for us. Prof. Song obtained his Ph.D. at Dartmouth working with the author, who has had collaborations with Central South University for several years and has hosted two exchange students in his laboratory for two years each.

Deformation Mechanisms

Three approaches will be used to examine the deformation mechanisms:

- *Post-mortem* TEM dislocation analysis will be performed using the Tecnai FEG TEM on specimens that have been crept at 973 K. Of particular interest is whether there has been a change in precipitate

size and spacing, and how these precipitates interact with dislocations. Previous reports on crept Laves-Phase-strengthened austenitic steels have suggested that the Laves phase precipitates become smaller during creep (Yamamoto et al., 2008).

- TEM *in-situ* straining experiments will be performed at 973 K in order to observe the fundamental dislocation/precipitate interactions directly. It is worth noting that if dislocation cutting of the precipitates occurs, this will likely lead to mechanical dissolution of the precipitates and their re-precipitation. The TEM *in-situ* straining studies will be performed on the Tecnai FEG TEM for which the P.I. has a Gatan single-tilt, hot-straining stage (operates to 1273 K) and a video system. Of particular interest is whether dislocations impinging on the grain boundary behave differently when they encounter a B2 precipitate rather than a Laves phase precipitate – as noted earlier, Tarigan et al. (2011, 2012) suggested that the role of the grain boundary Laves phase was to suppress deformation at the grain boundaries. It is important to correlate the *in-situ* straining experiments with the post-mortem TEM analysis. The latter can provide Burgers vector information, but always has the possibility that the dislocations have rearranged themselves (particularly after high temperature deformation) so that one does not see the real line direction of the gliding dislocations. It is worth noting that the P.I. has several year's experience with TEM *in-situ* straining experiments (Baker, Horton and Schulson, 1987; Baker, Schulson and Horton, 1987; Baker, Guha and Horton, 1993; Baker, and Horton, 1993; Baker et al., 1991; Baker and Liu, 1994; Horton, Baker and Yoo, 1991; Nagpal and Baker, 1991; Nagpal, Baker and Horton, 1994; Loudis and Baker, 2008; Liao and Baker, 2008; Liao and Baker, 2011a, 2011b), including recent work by Liao and Baker (2011a, 2011b) where TEM *in situ* straining observations were able to quantitatively explain the yield anomaly observed in Fe₂MnAl.

- We will use secondary electron imaging in a SEM to examine fracture surfaces.

Analysis of the Results

As an initial effort we will examine the creep model of Rösler and Artz (1990) for a particle-containing material. In this model, the strain rate, $\dot{\epsilon}$, at an applied stress of σ is described by

$$\dot{\epsilon} = CD \exp \left\{ -\frac{\mu b^2 r}{k_B T} \left[\left(1 - k \left(\frac{1 - \sigma}{\sigma_d} \right) \right)^2 \right]^3 \right\} \quad - (2)$$

where $C = 6\lambda\rho/b$, 2λ is the mean free path of a dislocation segment which has escaped from an obstacle (\sim the distance between particles), ρ is the dislocation density, b is the Burgers' vector, D is the self-diffusion coefficient, μ is the shear modulus, r is the particle radius, k_B is Boltzmann's constant, T is the temperature, k is the ratio of the line energy of a dislocation segment at a particle interface to its line energy in the matrix, and σ_d is $(1 - k^2)^{1/2} \sigma_{Or}$, where σ_{Or} is the Orowan stress to escape the particles. The question is which particles control the stress; the Laves phase precipitates, the B2 precipitates, the L1₂ precipitates or some combination of all three.

The P.I.'s has past experience in developing deformation models e.g. on the role of both grain boundaries and particles on the ductility of Intermetallic compounds (Baker and Schulson, 1989; Baker, 1999); a well-accepted model for the yield anomaly in B2 FeAl (George and Baker, 1998); and a model for strain-induced ferromagnetism in intermetallic compounds (Yang, Baker and Martin, 1999; Wu, Munroe and Baker, 2003).